NANO EXPRESS

Open Access

Electrospun Perovskite Nanofibers

Dongsheng Chen[1,2*] and Yanyan Zhu[1]

Abstract

$CH_3NH_3PbI_3$ perovskite nanofibers were synthesized by versatile electrospinning techniques. The synthetic $CH_3NH_3PbI_3$ nanofibers were characterized by X-ray diffraction, scanning electron microscopy, thermogravimetric analysis, and photoluminescence. As counter electrodes, the synthesized nanofibers increased the performance of the dye-sensitized solar cells from 1.58 to 2.09%. This improvement was attributed to the enhanced smoothness and efficiency of the electron transport path. Thus, $CH_3NH_3PbI_3$ perovskites nanofibers are potential alternative to platinum counter electrodes in dye-sensitized solar cells.

Keywords: $CH_3NH_3PbI_3$, Nanofibers, Electrospinning, Dye-sensitized solar cells

Background

Organic-inorganic hybrid materials have useful properties, such as plastic mechanical properties and good electronic mobility. Among these materials, semiconducting $CH_3NH_3PbI_3$ nanofibers attract considerable attention [1]. These nanofibers are currently being applied in sensitizers, hole-transporters, and combined absorber and electron transporter of nanostructured solar cells [1–3]. Spin-coating and vapor-assisted solution processes are often performed to produce perovskite thin films, and nontemplate synthesis of $CH_3NH_3PbBr_3$ perovskite nanoparticles is already reported [4–6]. Notably, perovskite-based hybrid solar cells exceed 15% efficiency with high reproducibility [2, 7].

Currently, dye-sensitized solar cells (DSSCs) have been extensively studied because of their availability and low cost [8]. In DSSCs, the counter electrode is usually platinum (Pt), which has excellent stability with regard to its catalytic activity. However, Pt is extremely expensive and has low abundance, and thus cannot be used in large-scale commercial applications [9].

One-dimensional (1D) nanofibers have attracted considerable attention because of their large length-to-diameter ratio, high surface area, excellent aspect ratio, and effective electronic properties [10]. Through the electrospinning technique, 1D nanofibers, such as TiO_2, ZnO, and Cu_2ZnSnS_4 (CZTS, 1.5 eV), can be used in solar cells [11–14]. Moreover, CZTS nanofibers can be used as replacements for counter electrodes to increase conversion efficiency [14]. Notably, the band gap and conductive type of $CH_3NH_3PbI_3$ perovskites are similar to those of CZTSs. Thus, we explore the use of $CH_3NH_3PbI_3$ perovskite nanofibers as counter electrodes in DSSCs.

As far as we know, we are the first to fabricate $CH_3NH_3PbI_3$ perovskite nanofiber using an electrospinning technique. We used polyvinylpyrrolidone (PVP) as an electrospinning medium. Subsequently, to explore the application of the synthesized nanofibers, we attempted to use them as a replacement for Pt in DSSCs.

Methods

Preparation of $CH_3NH_3PbI_3$ nanofiber

$CH_3NH_3PbI_3$ precursor was prepared by adding $CH_3NH_3I_3$ and PbI_2 at a ratio of 1:1 to 2 mL N,N-dimethylformamide (DMF) (J&K Scientific Ltd.). Approximately 0.25 g of PVP (K90, MW = 130000) was then dissolved into the solution. The resulting solution was stirred for 30 min until a homogeneous mixture was obtained. Facile electrospinning technique method was used to fabricate the PVP-$CH_3NH_3PbI_3$ perovskite nanofibers. The experimental procedure is schematically illustrated in Fig. 1. In the electrospinning process, the solution was injected through a stainless steel needle, which was connected to a high-voltage DC power supply. The solution was continuously fed through the nozzle using a syringe pump (LongerPump,TJ-3A/

* Correspondence: cds78@shiep.edu.cn
[1]College of Mathematics and Physics, Shanghai University of Electric Power, Shanghai 200090, China
[2]Department of Materials Science, Fudan University, Shanghai 200433, China

Fig. 1 Schematic diagram of the experimental procedure for $CH_3NH_3PbI_3$ nanofiber preparation
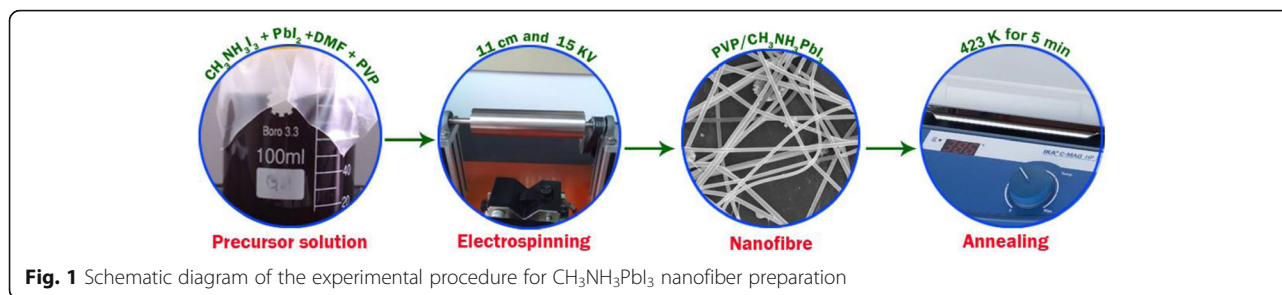
W0109-1B) at a rate of 10 µL/min. High voltage (15 kV) was applied between the needle and the grounded collector, which was situated 11 cm below the needle. As a result, a continuous stream was ejected from the nozzle and formed long fibers, which were subsequently collected. The $CH_3NH_3PbI_3$ nanofibers obtained were calcined at 150 and 200 °C separately in a nitrogen atmosphere for 5 min.

Characterization and Measurement

The phase structures of the prepared samples were characterized using an X-ray diffractometer (XRD, Bruker AX D8 Advance). Field-effect scanning electron microscope (Hitachi S-520) and transmission electron microscope were then used to study the microstructure of the samples (Tecnai G^2 F20, USA). Thermal analyses were performed through thermogravimetric analysis (TGA, model Perkin Elmer Pyris Diamond) in a nitrogenous atmosphere. The band gap was measured through the photoluminescence (PL) spectrum.

Results and Discussion
Phase Structures

Figure 2 shows the comparison between the XRD patterns of the $CH_3NH_3PbI_3$ perovskite nanofiber before annealing and those after annealing. Before annealing,

Fig. 2 XRD patterns of the $CH_3NH_3PbI_3$ nanofiber at different annealing temperatures
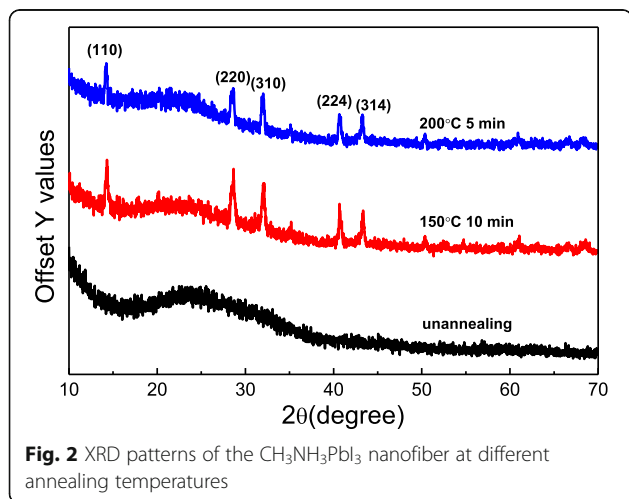
the synthetic nanofiber is amorphous. After the 5-min annealing treatment at 150 °C, the nanofibers are able to crystallize, and the main characteristic peaks are observed at 14.04°, 28.42°, 31.76°, 40.46°, and 43.02°, which correspond to the reflections from the (110), (220), (310), (224), and (314) crystal planes of the tetragonal perovskite structure. This result is consistent with the previously published results [15]. The best annealing temperature is 150 °C. When the temperature is further increased, the main characteristic peaks are slightly reduced.

Morphology

Figure 3a–c show the scanning electron microscopy (SEM) images of the $CH_3NH_3PbI_3$ perovskite nanofibers at different annealing temperatures. Figure 3a shows a wire-like network of $CH_3NH_3PbI_3$ perovskite nanofibers, which are covered throughout the surface. Moreover, the surfaces of $CH_3NH_3PbI_3$ nanofibers are quite smooth and their diameters ranges from 140 to 170 nm. Figure 3b indicates that the surfaces of the nanofibers roughened, and the diameters of the nanofibers are reduced when the nanofibers are annealed at 150 °C. When the annealing temperature is increased from 150 to 200 °C, the mesh nanofibers start to fracture and partly overlap one other (Fig. 3c). In addition, the structural features of the nanofibers exhibit a porous structure on the nanofiber wall, which contribute to the insertion of ion and facilitate its exit in the electrode material. Figure 3d indicates uniform nanocrystals. The selected area electron diffraction (SAED) image (Fig. 3e) exhibits diffraction rings corresponding to the (110), (220), and (310) directions of the $CH_3NH_3PbI_3$ nanofibers. The appearance of multiple diffraction rings is due to the random orientation of the polycrystallites. The spotty ring pattern with missing periodicity is due to the random orientation of the particles [16]. The results of the energy-dispersive (EDS) spectroscopy on the $CH_3NH_3PbI_3$ nanofibers after annealing treatment at 150 °C are shown in Fig. 3f. The nanofibers contain carbon, nitrogen, iodine, and lead, and have no impurity element. The compositions of the nanofiber are provided in the local compositions of C:N:H:Pb:I (0.9:0.8:4.5:1:2), which is extremely close to the stoichiometric $CH_3NH_3PbI_3$ perovskite.
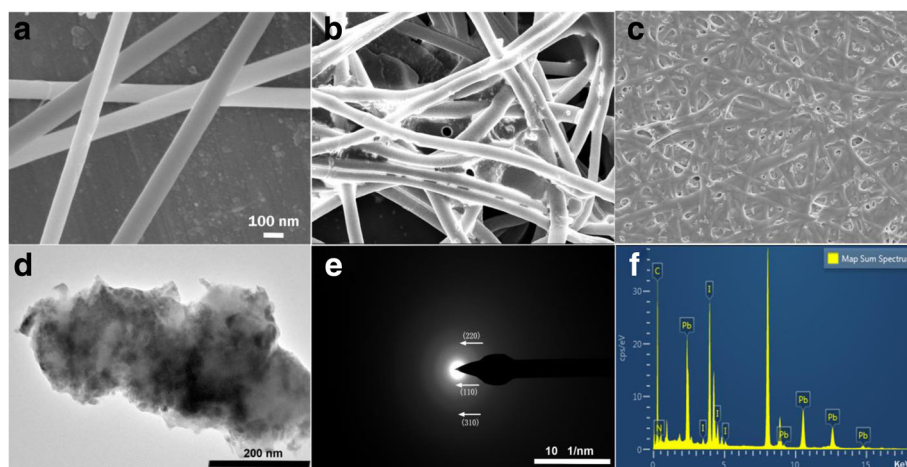
Fig. 3 a SEM images of the $CH_3NH_3PbI_3$ nanofiber, **b** and **c** SEM image after the 150 °C and 200 °C annealing treatments, **d** transmission electron microscopy image after the 150 °C annealing treatment, **e** SAED image, and **f** the EDS graph

Thermal Analysis

The TGA curves are shown in Fig. 4. The TGA curves have a heating rate of 20 °C/min under a N_2 atmosphere. The curve indicates that the thermal decomposition for the as-spun nanofibers is completed in two distinct steps. In the first step, the weight loss (3%) is observed between 25 and 200 °C. The loss is due to the evaporation of water and alcohol. In the second step, (200–400 °C), the weight loss is approximately 35% and is due to PVP degradation, which involves intra- and intermolecular transfer reaction mechanisms.

PL Spectroscopy

The band gap of the semiconductor plays an essential role in counter electrode of the DSSCs [9]. The PL spectra of $CH_3NH_3PbI_3$ nanofiber at different annealing temperatures is shown in Fig. 5. The peak is located mainly at 770 nm, indicating that the band gap is approximately l.61 eV, which is near the absorption band edge [17, 18]. At increasing temperature, the magnitude of the PL declines because of the increased fraction of the excitonic recombination. PL quenching is expected to originate from the charge-carrier extraction across the interface [19–21]. An efficient PL quenching indicates that the charge-carrier diffusion length inside the $CH_3NH_3PbI_3$ layer is comparable to the thickness of the layer [22].

Application of Counter Electrodes on the DSSCs

The $CH_3NH_3PbI_3$ nanofiber has been applied as a counter electrode in DSSCs. The DSSCs are each equipped with a TiO_2/FTO working electrode, redox couple (I^-/I^{3-}), and $CH_3NH_3PbI_3$/FTO counter electrodes [14]. The current-voltage (J – V) characteristics are measured using Pt/FTO and $CH_3NH_3PbI_3$/FTO counter electrodes. Figure 6 and Table 1 demonstrate that the open circuit voltage (V_{OC}), short circuit current density
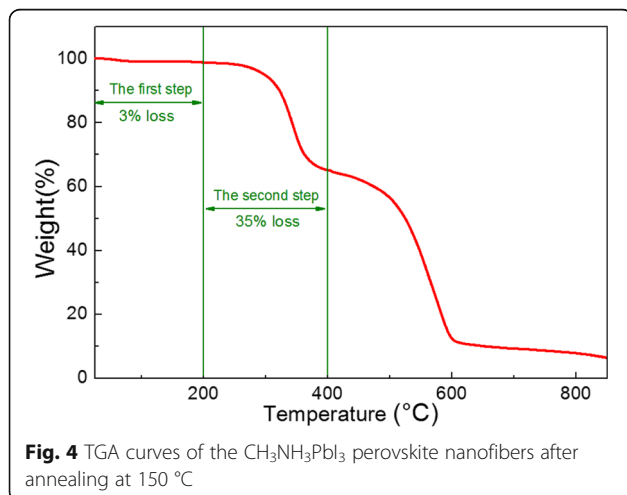
Fig. 4 TGA curves of the $CH_3NH_3PbI_3$ perovskite nanofibers after annealing at 150 °C
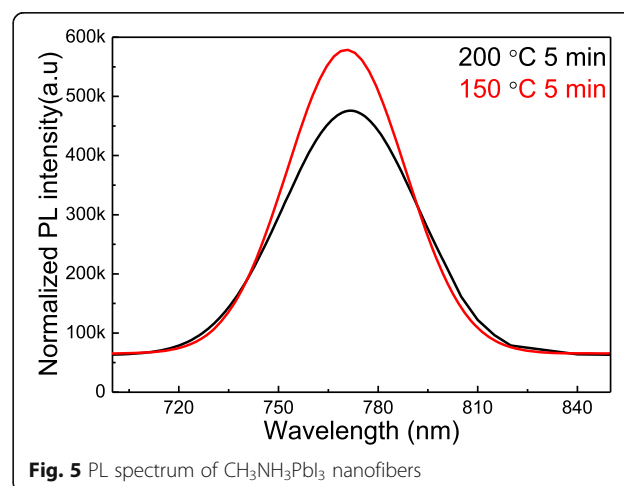
Fig. 5 PL spectrum of $CH_3NH_3PbI_3$ nanofibers
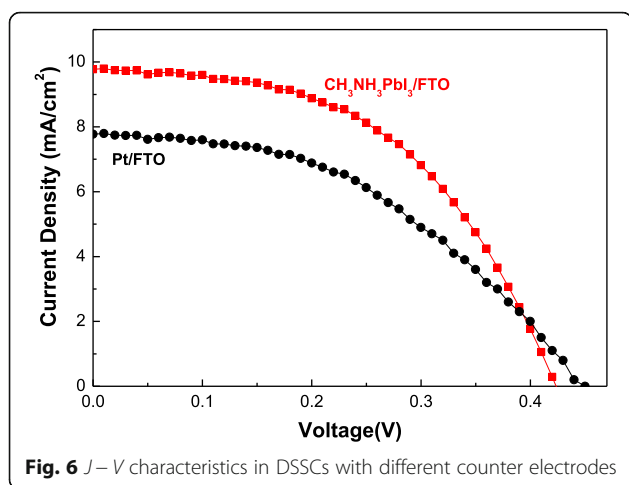
Fig. 6 *J − V* characteristics in DSSCs with different counter electrodes

(J_{SC}), and filled factor (FF) of the device are 0.45 V, 7.78 mA/cm², and 45%, respectively. When the counter electrodes have been changed from Pt/FTO to $CH_3NH_3PbI_3$/FTO, the J_{SC} and FF values have increased slightly by 9.81 mA/cm² and 51%, respectively. Moreover, the conversion efficiency of the device has increased from 1.58 to 2.09% because of the improved efficiency of the electron transport path in the $CH_3NH_3PbI_3$/FTO electrodes. Meanwhile, the nanofibers with large surface areas contribute to the redox reaction between the counter electrode and the electrolyte, and thus, a decreased interfacial recombination in the DSSCs is observed [14].

Conclusions

In summary, we successfully synthesized $CH_3NH_3PbI_3$ nanofibers with diameters ranging from 140 to 170 nm via electrospinning technique. The XRD analysis results revealed that the synthetic nanofibers contained the pure phase of $CH_3NH_3PbI_3$ perovskites with good crystallinity. The PL properties demonstrated that the nanofibers have a band gap energy of approximately 1.6 eV. When the nanofibers were used to the counter electrodes of the DSSCs, the conversion efficiency of the device increased from 1.58 to 2.09% because of the large surface area of the small nanofibers. Thus, our synthetic method can significantly contribute to low-cost and large-scale preparation of nanofibers for actual photovoltaic applications.

Table 1 Photovoltaic performances of the DSSCs with different counter electrodes

The electrodes	Voc (V)	J_{sc} (mA/cm²)	FF (%)	Eta (%)
Pt/FTO	0.45	7.78	45	1.58
$CH_3NH_3PbI_3$/FTO	0.42	9.80	51	2.09

Abbreviations

DMF: N,N-Dimethylformamide; PL: Photoluminescence; PVP: Polyvinylpyrrolidone; SAED: Selected area electron diffraction; SEM: Scanning electron microscopy; TGA: Thermogravimetric analysis; XRD: X-ray powder diffraction

Authors' contributions

DC conceived and designed the study, performed the experiments, and wrote the paper. YZ suggested the added experiments, revised the paper, and provided the fees for the published paper. Both authors read and approved the manuscript.

Competing interests

The authors declare that they have no competing interests.

References

1. Kojima A, Teshima K, Shirai Y, Miyasaka T (2009) Organometal halide perovskites as visible-light sensitizers for photovoltaic cells. J Am Chem Soc 131:6050–6051
2. Chung I, Lee B, He J, Chang RPH, Kanatzidis MG (2012) All-solid-state dye-sensitized solar cells with high efficiency. Nature 485:486–489
3. Lee MM, Teuscher J, Miyasaka T, Murakami TN, Snaith HJ (2012) Efficient hybrid solar cells based on meso-superstructured organometal halide perovskites. Science 338:643–647
4. Dualeh A, Moehl T, Tétreault N, Teuscher J, Gao P, Nazeeruddin MK, Grätzel M (2014) Impedance spectroscopic analysis of lead iodide perovskite-sensitized solid-state solar cells. ACS Nano 8:362–373
5. Chen Q, Zhou H, Hong Z, Luo S, Duan H-S, Wang H-H, Liu Y, Li G, Yang Y (2014) Planar heterojunction perovskite solar cells via vapor-assisted solution process. J Am Chem Soc 136:622–625
6. Schmidt LC, Pertegas A, González-Carrero S, Malinkiewicz O, Agouram S, Mínguez Espallargas G, Bolink HJ, Galian RE, Perez-Prieto J (2014) Nontemplate synthesis of CH3NH3PbBr3 perovskite. J Am Chem Soc 136:850–853
7. Conings B, Baeten L, De Dobbelaere C, D'Haen J, Manca J, Boyen H-G (2014) Perovskite-based hybrid solar cells exceeding 10% efficiency with high reproducibility using a thin film sandwich approach. Adv Mater 26:2041–2046
8. Santra PK, Kamat PV (2012) Mn-Doped quantum dot sensitized solar cells: a strategy to boost efficiency over 5%. J Am Chem Soc 134:2508–2511
9. Ramasamy K, Tien B, Archana PS, Gupta A (2014) Copper antimony sulfide (CuSbS2) mesocrystals: a potential counter electrode material for dye-sensitized solar cells. Mater Lett 124:227–230
10. Mali SS, Kim H, Jang WY, Park HS, Patil PS, Hong CK (2013) Novel synthesis and characterization of mesoporous ZnO nanofibers by electrospinning technique. ACS Sustainable Chem Eng 1:1207–1213
11. Jung YH, Park KH, Oh JS, Kim DH, Hong CK (2013) Effect of TiO2 rutile nanorods on the photoelectrodes of dye-sensitized solar cells. Nanoscale Res Lett 8:37–42
12. Song W, Wang Y, Zhao B (2007) Surface-enhanced Raman scattering of 4-mercaptopyridine on the surface of TiO2 nanofibers coated with Ag nanoparticles. J Phys Chem C 111:12786–12791
13. Choi S-H, Ankonina G, Youn D-Y, Seong-Geun O, Hong J-M, Rothschild A, Kim I-D (2009) Hollow ZnO nanofibers fabricated using electrospun polymer templates and their electronic transport properties. ACS Nano 3:2623–2631
14. Mali SS, Patil PS, Hong CK (2014) Low-cost electrospun highly crystalline kesterite Cu2ZnSnS4 nanofiber counter electrodes for efficient dye-sensitized solar cells. ACS Appl Mater Interfaces 6:1688–1696
15. Baikie T, Fang Y, Kadro JM, Schreyer M, Wei F, Mhaisalkar SG, Gratzel M, White JT (2013) Synthesis and crystal chemistry of the hybrid perovskite (CH3NH3)PbI3 for solid-state sensitised solar cell applications. J Mater Chem A 1:5628–5641

16. Rajesh G, Muthukumarasamy N, Subramanian EP, Venkatraman MR, Agilan S, Ragavendran V, Thambidurai M, Velumani S, Junsin Y, Dhayalan V (2015) Solution-based synthesis of high yield CZTS (Cu_2ZnSnS_4) spherical quantum dots. Superlattice Microst 77:305–312

17. Chen Z, Yu CL, Shum K, Wang JJ, Pfenninger W, Vockic N, Midgley J, Kenney JT (2012) Photoluminescence study of polycrystalline $CsSnI_3$ thin films: determination of exciton binding energy. J Lumin 132:345–349

18. Park N-G (2013) Organometal perovskite light absorbers toward a 20% efficiency low-cost solid-state mesoscopic solar cell. J Phys Chem Lett 4: 2423–2429

19. Lian HJ, Yang A, Thewalt MLW, Lauck R, Cardona M (2006) Effects of sulfur isotopic composition on the band gap of PbS. Phys Rev B 73:233202

20. Lunt RR, Benziger JB, Forrest SR (2010) Relationship between crystalline order and exciton diffusion length in molecular organic semiconductors. Adv Mater 22:1233–1236

21. Shaw PE, Ruseckas A, Samuel IDW (2008) Exciton diffusion measurements in poly (3- hexylthiophene). Adv Mater 20:3516–3520

22. Xing G, Mathews N, Sun S, Lim SS, Lam YM, Grätzel M, Mhaisalkar S, Sum TC (2013) Long-range balanced electron- and hole-transport lengths in organic-inorganic $CH_3NH_3PbI_3$. Science 342:344